Cure Kinetics and Rheology Characterization of Soy-Based Epoxy Resin System

G. Liang, K. Chandrashekhara

Department of Mechanical and Aerospace Engineering, University of Missouri-Rolla, Rolla, Missouri 65409

ABSTRACT: A novel soy-based epoxy resin system was synthesized by the process of transesterification and epoxidation of regular soy bean oil, which has the potential to be widely usable in various composite manufacturing processes. Cure kinetics and rheology are two chemical properties commonly required in process modeling. In this work, the cure kinetics and rheology of the soy-based resin system were measured by means of differential scanning calorimetry (DSC) and viscometer. DSC was used to measure the heat flow of dynamic and isothermal curing processes. The cure kinetics models of the different formulations were thus developed. A Brookfield viscometer was used to measure the change in viscosity under isothermal conditions. A novel neural network-based model was developed to improve modeling accuracy. The models developed for cure kinetics and rheology for soy-based epoxy resin system can be readily applied to composite processing. © 2006 Wiley Periodicals, Inc. J Appl Polym Sci 102: 3168–3180, 2006

Key words: soy-based resin; cure kinetics; rheology; neural network

INTRODUCTION

Fiber-reinforced polymer (FRP) composite materials possess superior properties, such as high strength and stiffness-to-weight ratio, resistance to environmental deterioration, high electrical insulation, and low assembly cost. However, high material cost compared to conventional materials has led to their limited applications. Therefore, the low-cost fiber-reinforced composites from renewable resources such as unsaturated triglyceride oils are gaining great interest in the area of composite materials. Among the renewable triglyceride oils, soybean oil is attracting more and more attention for industrial applications because it is readily available and offer relatively low cost.

Epoxidized allyl soyate (EAS) was developed at the University of Missouri-Rolla by the process of transesterification and epoxidation of regular soy bean oil. This soy-based epoxy resin system possesses higher reactivity than the commercially available ESO, and is more inclined to form intermolecular crosslinking, which shows great potential for EAS as the ideal substitute for conventional epoxy resin used in composite industry. Results indicate that EAS has improved properties when used in pultrusion process for low levels of soyate resin content.[1–3] EAS also has the potential to be used in other composite manufacturing methods like resin transfer molding (RTM) and vacuum-assisted resin transfer molding (VARTM).

Numerical process modeling has been recognized as an important tool in the development of cost-effective composite manufacturing techniques. It can provide useful information in the selection of appropriate temperatures, pressures, and other related parameter settings during the cure of polymer matrix composites. Appropriate parameter setting will eventually improve the composite product quality. Process modeling of composite manufacturing techniques has been the focus of research work in recent years.

Cure kinetics and rheology are the two key chemical properties commonly required in numerical simulations of polymer composite manufacturing processes. Cure kinetics of a thermosetting resin correlates heat release rate with the temperature and the degree of cure, and can be directly applied into formulation of heat transfer and heat generation models. Rheology provides information on viscosity change along with curing process, and therefore, is critical in modeling of resin flow in various composite manufacturing processes.

Phenomenological modeling (also called empirical modeling) approach is commonly used to obtain analytical expressions for cure kinetics and viscosity, and it has been proved an effective approach with simple procedure and satisfactory accuracy. In phenomeno-

logical modeling the chemical details of the reacting system are ignored and an approximated relationship is applied according to the reaction type, and then the parameters in the mathematical model are fitted with experimental data. Lee et al.[4] investigated the cure kinetics and viscosity of Hercules 3501–6 resin. The cure kinetics was expressed in a modified Arrhenius-type equation, and the viscosity was fitted in an expression in terms of temperature and degree of cure, which was found to be in good agreement with the experimental data in this case. Dusi et al.[5] measured and modeled the cure kinetics and viscosity of Fiberite 976 Resin. Shanku et al.[6] reported the rheological characteristics and cure kinetics of Epon 862/W epoxy resin for pultrusion use; the viscosity expression used in previous investigations was modified to a quadratic form in this case. A number of other resins curing properties have also been studied by researchers, such as 8552 epoxy resin by Hubert et al.,[7] ICI Fiberite 977–3 and 977–2 by Mantell et al.,[8] AS4/3501–6 Graphite-Epoxy Prepregs by Kim et al.,[9] and an epoxy/anhydride system by Ivankovic et al.[10] It can be seen that the curing behavior is different for different resin systems. Consequently, a variety of phenomenological models for cure kinetics and rheology have been proposed for different resin systems in the literature. The analytical models of cure kinetics and rheology have found wide applications in numerical simulations of composite manufacturing processes.[3,11–15] In our previous study,[1–3] the focus was on the curing of soy composites with amine curing agent. Only 30% EAS could be used in these formulations. However, the cure kinetics and the rheology studies were not performed in detail.

In the present work, high levels of soyate resin content (up to 75% EAS) was used with anhydride as the curing agent. The cure kinetics and rheological characteristics of the soy-based epoxy system were studied. The cure kinetics models of the different formulations were developed. The rheology was measured with a Brookfield viscometer and was characterized using neural network.

CURE KINETICS AND RHELOLOGY MODELS

Cure kinetic models

The cure process of a thermosetting resin results in conversion of low-molecular-weight monomers or prepolymers into a highly crosslinked, three-dimensional macromolecular structure. The degree of cure, α, is generally used to indicate the extent of the resin chemical reaction. The α is proportional to the amount of heat given off by bond formation, and is usually defined as:

$$\alpha = \frac{H}{H_U} \qquad (1)$$

where H is the accumulative heat of reaction up to a given time t during the curing process, and H_U is the ultimate heat released during a complete reaction. For an uncured resin, $\alpha = 0$, whereas for a completely cured resin, $\alpha = 1$.

The curing rate is assumed to be proportional to the rate of heat generation and is calculated by the following expression:

$$\frac{d\alpha}{dt} = \frac{1}{H_U}\left(\frac{dH}{dt}\right) \qquad (2)$$

A number of phenomenological models for cure kinetics have been developed to characterize the curing process for different resin systems. The simplest one is the nth-order rate equation:

$$\frac{d\alpha}{dt} = K(1 - \alpha)^n \qquad (3)$$

$$K = K_0 \exp\left(-\frac{\Delta E_A}{RT}\right)$$

where n is the reaction order, and K is the reaction rate constant, which is an Arrhenius function of temperature, K_0 is the pre-exponential constant or Arrhenius frequency factor, ΔE_A is the activation energy, R is the universal gas constant, and T is the absolute temperature. The nth-order kinetics model does not account for any autocatalytic effects and so it predicts maximum reaction rate at the beginning of the curing.

For autocatalytic thermosetting resin systems, the following equation has been applied:

$$\frac{d\alpha}{dt} = K\alpha^m(1 - \alpha)^n \qquad (4)$$

where m and n are reaction orders to be determined by experimental data, and K has the same definition as in eq. (3). Rather than at the beginning of the reaction process as in eq. (3), the maximum reaction rate takes place in the intermediate conversion stage for eq. (4), which results in a bell-shaped reaction rate versus time curve for an autocatalytic reaction process.

Both the nth-order and autocatalytic model use a single rate constant to model the whole curing process. In practice, multiple events may occur simultaneously and lead to very complicated reaction; consequently, the use of multiple rate constants can provide more accurate modeling results. Kamal's model[16] involves two rate constants and has been applied successfully to model a variety of resins,

$$\frac{d\alpha}{dt} = (K_1 + K_2\alpha^m)(1 - \alpha)^n \qquad (5)$$

$$K_i = K_{i0}\exp(-\Delta E_i/RT) \quad (i = 1,2)$$

where ΔE_i are activation energies, R is the universal gas constant, m and n are material constants to be determined by experimental data, and K_1 and K_2 have the same definition as in eq. (3).

The various mathematical models described above have been widely used. However, their validity is limited to reactions for which the kinetics of bond formation is the only rate-controlling step in the curing process. While this is usually true in the early stage, other factors may come into play as reactants are consumed and crosslinking network is formed. As a consequence, species diffusion can become very slow and govern the curing reaction rate near and above the glass transition. To account for the different cure rate controlling mechanisms and to achieve greater accuracy at high conversions, some modifications on the available cure kinetics models have been introduced.

Cole[17] modified the species eq. (4) by adding a term to explicitly account for the shift from kinetics to diffusion control in an autocatalytic thermosetting resin system; the modified expression has the following form:

$$\frac{d\alpha}{dt} = \frac{K\alpha^m(1-\alpha)^n}{1 + e^{C\{\alpha-(\alpha_{C0}+\alpha_{CT}T)\}}} \quad (6)$$

where C is the diffusion constant, α_{C0} is the critical degree of cure at absolute zero temperature. The constant α_{CT} accounts for an increase in critical resin degree of cure with temperature. K, m, and n follow the same definitions as in previous equations.

One modified form of Kamal's model has been proposed as:

$$\frac{d\alpha}{dt} = (K_1 + K_2\alpha^m)(\alpha_{\max} - \alpha)^n \quad (7)$$

where $\alpha_{\max}$ is the maximum degree of cure at a given temperature due to the vitrification phenomenon observed in isothermal cure. The constants m and n are reaction orders to be experimentally determined, while K_1 and K_2 are the same as in eq. (5).

The modified Kamal model incorporates the term $\alpha_{\max}$, so that the fractional conversion will not exceed the degree of cure associated with vitrification at the specific temperature.

Rheology models

The viscosity of a curing resin system is determined by two factors: the degree of cure and the temperature. As the cure proceeds, the molecular size increases and so does the crosslinking density, which decrease the mobility and hence increase the viscosity of the resin system. On the other hand, the temperature exerts a direct effect on the dynamics of molecules and so the viscosity.

Much work has been done to develop appropriate mathematical models for the descriptions of the viscosity advancements for various thermosetting resins during cure. The following empirical model finds the most common applications:

$$\mu = \mu_\infty \exp\left(\frac{U}{RT}\right)\exp(K_0\alpha) \quad (8)$$

where μ_∞ is a constant, U is the activation energy for viscosity assumed to be independent of the degree of cure α, and K_0 is a constant assumed to be independent of temperature. R is the universal gas constant and T is the temperature.

Shanku et al.[6] modified eq. (8) to a quadratic form to account for the nonlinear relation between the logarithm of the viscosity and the degree of cure of Epon 862/W epoxy system,

$$\mu = \mu_\infty \exp\left(\frac{U}{RT} + K_1\alpha + K_2\alpha^2\right) \quad (9)$$

where K_1 and K_2 are two parameters which are both temperature dependent. The other symbols are same as in eq. (8).

A more complex empirical model proposed by Kenny et al.[18] represents more comprehensively the effect of the degree of cure on the resin viscosity by accounting for the degree of cure at gelation,

$$\mu = A_\mu \exp\left(\frac{E_\mu}{RT}\right)\left[\frac{\alpha_g}{\alpha_g - \alpha}\right]^{(A+B\alpha)} \quad (10)$$

where A_μ, E_μ, A and B are experimentally determined constants, R is the universal gas constant, and α_g is the degree of cure at gelation. In this expression, it can be seen that as α approaches α_g, the resin viscosity increases dramatically as the polymer system becomes a three-dimensional network.

Other than the viscosity models listed above, Williams–Landel–Ferry equation (WLF)[19] and its modifications have also found extensive application in viscosity modeling. The WLF equation has the following well-known form:

$$\ln\frac{\eta(T)}{\eta_g} = \frac{C_1(T - T_{g0})}{C_2 + T - T_{g0})} \quad (11)$$

where η_g is the viscosity at the glass transition, T_{g0} is the glass-transition temperature of the uncured resin system, and C_1 and C_2 are constants independent of temperature. The increase of the glass-transition tem-

perature due to network formation is incorporated into the WLF equation.

Neural network-based rheology model

For both cure kinetics and viscosity characterization by phenomenological approach, an appropriate type of empirical model is first postulated, and then the material constants present in the mathematical model are determined by the experimental data with some numerical fitting algorithms.

In the present study, the authors found that, while the cure kinetics of the soy-based epoxy resins can be well described by the Kamal's kinetic model, none of the viscosity models available in literature describe the rheological characteristics of the soy-based epoxy resin system to satisfaction. An important reason is that only a limited number of empirical models are available. For a specific resin system, it may turn out that all the available empirical models can not fit the test data accurately. In this work, a novel method for modeling viscosity of thermosetting resins based on neural network was developed to improve the modeling accuracy and to improve the process modeling eventually.

The foundation of neural network research is well summarized by Anderson and Rosenfeld[20] and Lau.[21] There is tremendous renewed interest in neural network in the last decade or so and neural networks have been widely used in different areas.[22–24] It has been shown that two-layer feedforward neural networks, with sigmoid transfer functions in the hidden layer and linear transfer functions in the output layer, can approximate virtually any function of interest to any degree of accuracy, provided sufficient hidden units are available.[25–27]

Figure 1 illustrates the feedforward neural network structure used in this work. It has one input layer, one hidden layer, and one output layer. The inputs to the neural network are the degree of cure, α, and the resin temperature, T. The output is the corresponding viscosity μ. The W's and B's are the weights and biases of the neural network, respectively. Their values are fully determined by the training process. The activation function of the hidden layer can be either the log sigmoid function

$$f(x) = \frac{1}{1 + e^{-x}} \tag{12}$$

or the tangent sigmoid function

$$f(x) = \frac{e^x - e^{-x}}{e^x + e^{-x}} \tag{13}$$

The activation function of the output layer is the identity function, $f(x) = x$. Thus, given the inputs α and T, the viscosity μ is expressed as
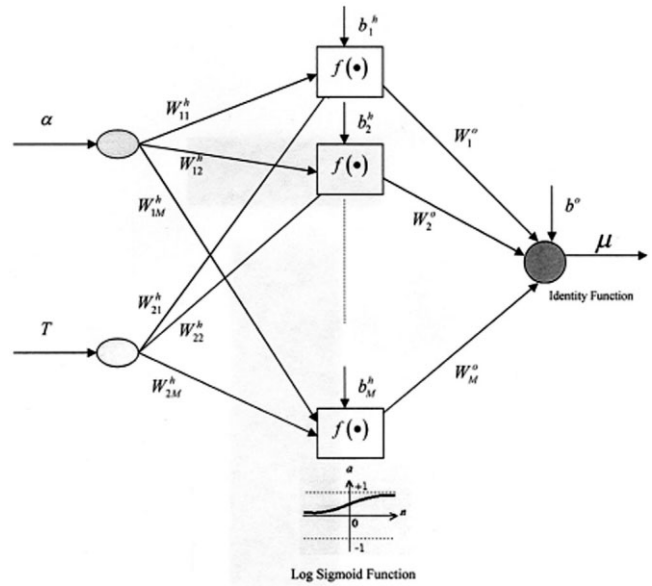

Figure 1 Structure of the feedforward neural network.

$$\mu = \sum_{j=1}^{N} W_j^0 f(O)_j + b^0 \tag{14}$$

$$O_j = \{\alpha, T\}, \left\{ \begin{array}{c} W_{1j}^h \\ W_{2j}^h \end{array} \right\} + b_j^h$$

where N is the number of neurons in the hidden layer of the neural network. The value of N can be changed to optimize the performance of the neural network.

The neural network is trained by the experimental data. Since no specific form is assumed at the beginning, the function of viscosity is determined by the experimental data and the neural network structure. The curve fitting process is then simplified to choosing the number of the neurons in the hidden layer. By varying the number of the neurons in the hidden layer and the initial weights and biases in the neural network, satisfactory curve fitting of the experimental data can be achieved. The expressions obtained above for the viscosity can be readily applied in process modeling of various composite manufacturing methods.

EXPERIMENTAL

Materials

The base epoxy resin used in the study was Shell Epon® 9500 (Shell Chemical Co., Houston, TX). Lindride® LS 56V (Lindau Chemicals, Columbia, SC) was the anhydride curing agent used. Soy-based resin was synthesized in a two-step laboratory scale process from regular food-grade soybean oil. At first the triglycerides molecules in the soybean oil were transesterified with allyl alcohol to yield fatty acid allyl es-

Resin formulation	Total heat of reaction H_U (J/g) at heating rates of				Average H_U (J/g)
	2°C/min	5°C/min	10°C/min	20°C/min	
Epon	301.0	313.6	306.8	303.4	306.2
EAS25	278.8	280.8	288.9	281.0	282.4
EAS50	240.1	225.0	208.5	226.9	225.1
EAS75	203.1	192.7	199.4	181.6	194.2

ters. Next the fatty acid esters were epoxidized using benzoyl peroxide to yield soyate epoxy resin. Four resin formulations, Epon (Shell Epon 9500), EAS25 (25% EAS + 75% Shell Epon 9500), EAS50 (50% EAS + 50% Shell Epon 9500), and EAS75 (75% EAS + 25% Shell Epon 9500), were characterized. The weight ratio of resin to curing agent was 100 : 70.

Differential scanning calorimetry measurements

Differential scanning calorimetry (DSC) is an extensively used experimental tool for thermal analysis by detection of heat flows from the samples. It is the most commonly used device to characterize cure kinetics for thermosetting polymer resins. The heat of reaction, the rate of cure, and the degree of cure can be measured by DSC. The experiments are categorized in two typical modes: (1) isothermal scanning, during which the test is performed with the sample kept at a constant temperature; and (2) dynamic scanning, during which the sample is heated at a constant scanning rate.

In this work, a Model 2010 DSC (by TA Instruments) is used to study the cure kinetics of the four formulations of soy-based epoxy resins. Resin samples weighing ~5–10 mg were encapsulated in aluminum hermetic pans and then subjected to isothermal calorimetry and dynamic DSC scanning.

Dynamic runs at four different heating rates of 2, 5, 10, and 20°C/min were made to determine the conversion profiles and the total heats released during the dynamic curing for all the four epoxy formulations. The prepared resin samples were placed in the DSC furnace at ambient temperature, and then cooled to 0°C with liquid nitrogen as the coolant. The heat evolutions are then monitored from 0°C to 250°C for each heating rate. The total reaction heat is then evaluated by

$$H_U = \int_0^{t_{fd}} \left(\frac{dQ}{dt}\right)_d dt \tag{15}$$

where t_{fd} is the time required for the completion of the chemical reaction during the dynamic scanning, and $(dQ/dt)_d$ is the instantaneous heat flow during the dynamic scanning. The integration baseline was obtained by drawing a straight line connecting the baseline before and after the heat flow peak.

As expected, for each resin formulation, lower heating rates result in lower onset temperature of reaction,
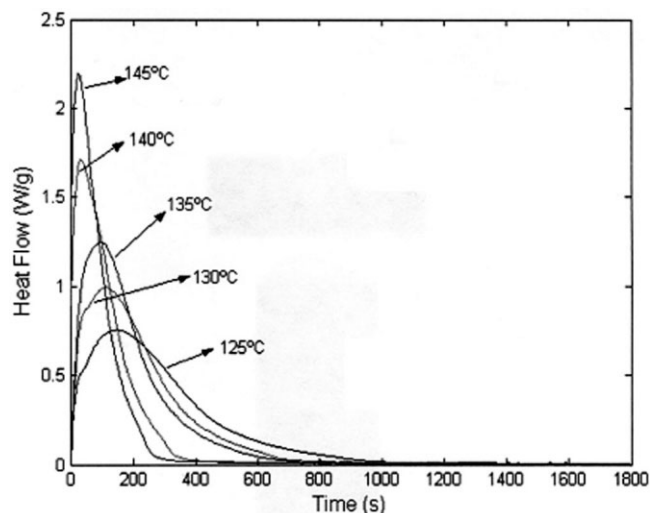

Figure 2 Heat flow versus time at different curing temperatures for Epon.
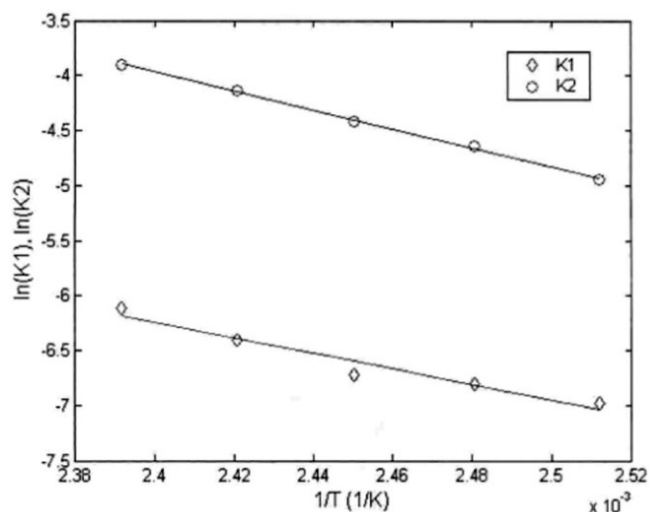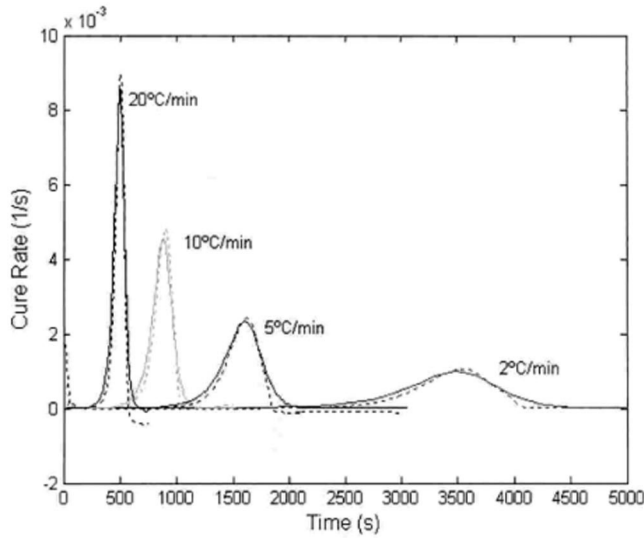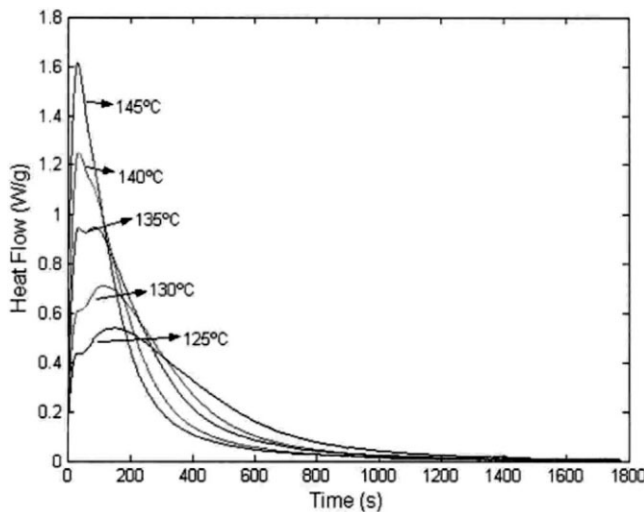

Figure 3 Arrhenius plots of the isothermal reaction rate constants for Epon.
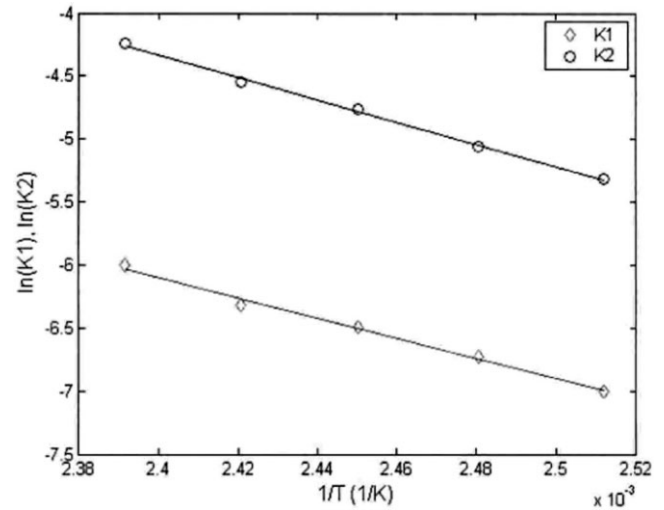
Figure 4 Comparison of experimental data (–) with the kinetic model data (−) at different heating rates for Epon, with zero time corresponding to the 0 °C temperature.

Figure 6 Arrhenius plots of the isothermal reaction rate constants for EAS25.

while different heating rates give consistent total reaction heats for a certain resin formation. The total reaction heats for the four epoxy resin formulations, Epon, EAS25, EAS50, and EAS75, are listed in Table I.

In accordance with the dynamic curing profiles obtained previously, five temperatures, 125°C, 130°C, 135°C, 140°C, and 145°C, are selected for the isothermal DSC experiments for each epoxy resin formulation. Thermal curves are recorded until the rate of heat flow approaches zero. The heat flow rates of all the four resin formulations are found to approximate zero within 30 min during the isothermal scans. The amount of heat released up to time t in an isothermal measurement is determined by

$$H = \int_0^t \left(\frac{dQ}{dt}\right) dt, \qquad (16)$$

where dQ/dt is the instantaneous heat flow during the isothermal scanning.

After each isothermal scan, the sample was rapidly cooled in the DSC cell to 0°C and then reheated at 10°C/min to 250°C to determine the glass-transition temperature (T_g) and the residual heat of reaction. The glass-transition temperature is reported as the midpoint temperature of the extrapolated endothermic shifts observed during the re-scans. The glass-transition temperatures from the different isothermal scans

Figure 5 Heat flow versus time at different curing temperatures for EAS25.
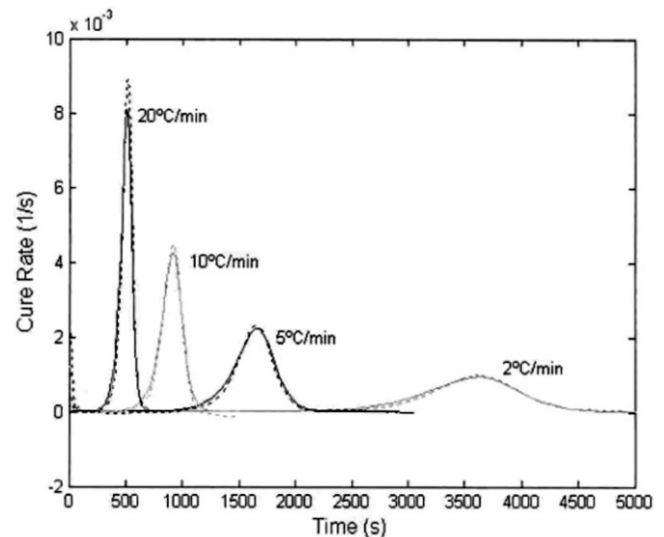
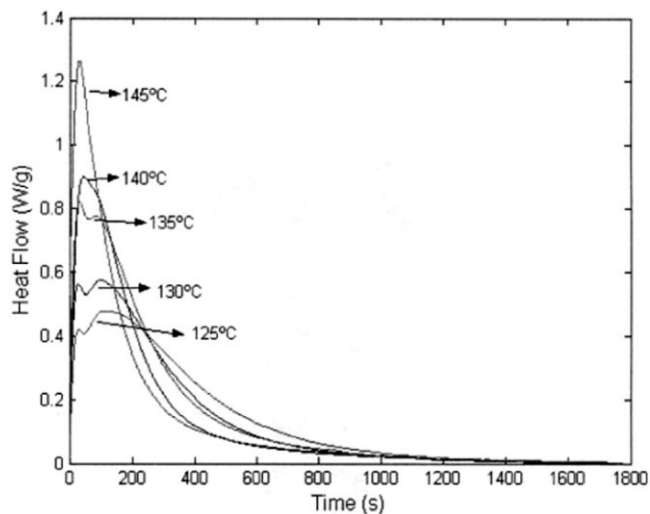**Figure 7** Comparison of experimental data (–) with the kinetic model data (−) at different heating rates for EAS25, with zero time corresponding to the 0 °C temperature.

Figure 8 Heat flow versus time at different curing temperatures for EAS50.

Figure 10 Comparison of experimental data (–) with the kinetic model data (−) at different heating rates for EAS50, with zero time corresponding to the 0 °C temperature.
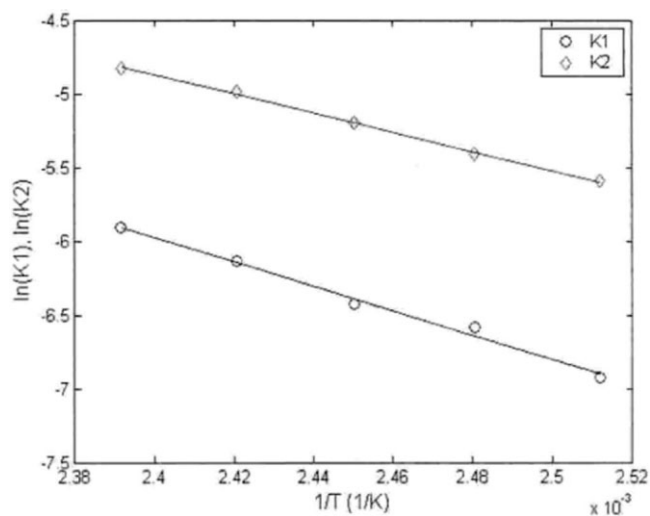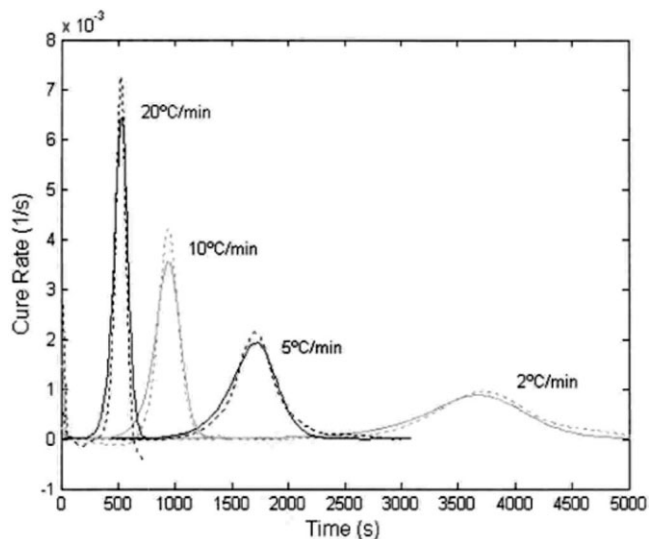
are constant for each resin formulation. By taking the average value, the T_g for Epon is found to be 108.2°C. As the soy-based epoxy resin concentration increases, the T_g drops. The T_g's of all the four resin formulations are lower than the isothermal scanning temperatures even when they are completely cured; so the vitrification phenomenon reported in the literature[5,7,9,10,15] is not applicable for the resin system in the present study. Consequently, the curing process will not be impeded by the lack of molecular mobility.

Viscosity measurements

Viscosity instruments have been widely accepted as reliable tools for obtaining meaningful rheological measurements on thermosetting polymer resins. As

for cure kinetics, the viscosity measurements can also be categorized as dynamic viscosity measurement, during which the temperature of the resin is changed according to some special cure cycle, and isothermal viscosity measurement, during which the temperature of the resin is kept constant. The time–temperature history of viscosity is recorded and then applied in the viscosity modeling.

A Brookfield LVDV-II+ programmable rotational-type viscometer is used to perform isothermal viscosity measurements at the temperatures of 125°C, 130°C, 135°C, 140°C, and 145°C, the identical isothermal temperatures as utilized for DSC measurements. For a given viscosity, the viscous resistance is related to the

Figure 9 Arrhenius plots of the isothermal reaction rate constants for EAS50.
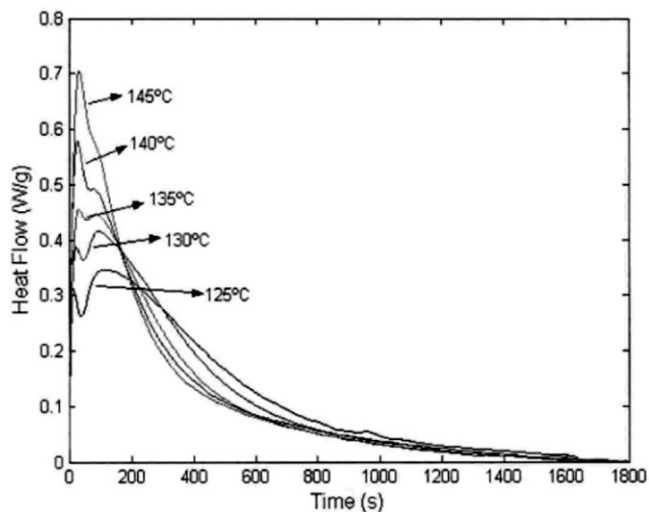
Figure 11 Heat flow versus time at different curing temperatures for EAS75.

Figure 12 Arrhenius plots of the isothermal reaction rate constants for EAS75.
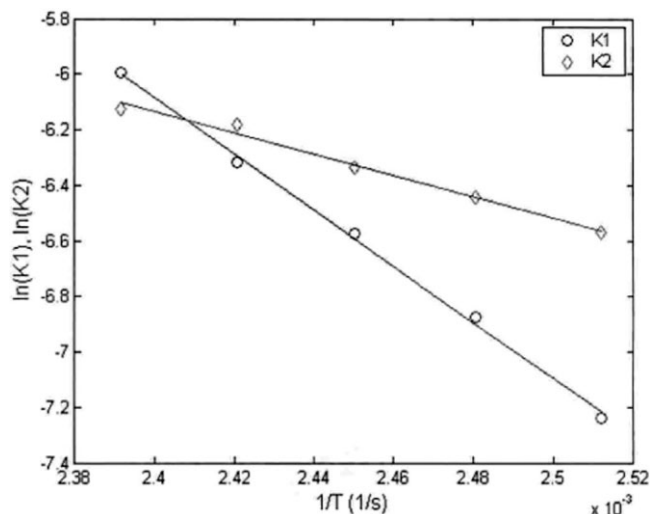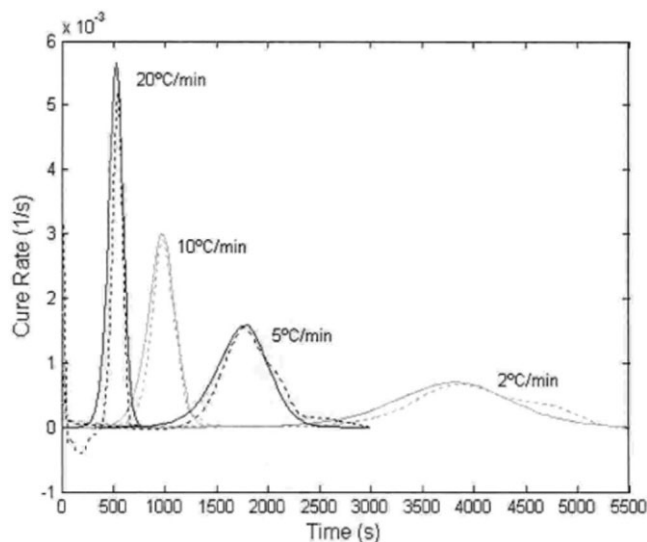

Figure 13 Comparison of experimental data (–) with the kinetic model data (−) at different heating rates for EAS75, with zero time corresponding to the 0 °C temperature.

spindle rotational speed and the spindle geometry. In this study, the spindle used is disposable SC4–27, and the chamber used is disposable HT-2DB, both of them are specially designed for measuring sticky fluids. The clearance between the spindle periphery and the chamber inner wall is 3.15 mm. The viscosity histories, up to 10 Pa s, at different temperatures for each resin formulation are recorded with time. Three consecutive viscosity ranges are applied to ensure enough accuracy for each measurement.

The resin sample temperature was controlled by a lab-made heating device. The heating device consisted of a heating cord, a thermocouple, and a temperature controller. The heating cord can be wrapped around the chamber to heat the resin. The thermocouple measures the real-time temperature of the resin in the chamber and provides feedback to the temperature controller. The temperature controller controls the electric power to the heating cord by monitoring the resin temperature. The resin sample in the chamber is thus controlled at a certain temperature. The heating device can heat the resin to the set temperature in less than 1 min, and the degree of cure of the resin sample is therefore assumed to be zero at the start of the

viscosity recording. The temperature control accuracy is observed to be ±1°C.

RESULTS AND DISCUSSION

Cure characterization

Different models have been used for the cure kinetics modeling of the epoxy/anhydride polymerization, for example, Woo and Seferis[28] modeled a DGEBA/TMA resin system with the nth-order rate equation [see eq. (3)], and the value of n changes as the curing proceeds; Khanna and Chanda[29] reported that, with the inclusion of a diffusion factor into a semiempirical autocatalytic model, the cure kinetics of an epoxy/anhydride resin system was predicted with precision; and Ivankovic et al.[10] used a modified Kamal's equation to model the kinetic behavior of an epoxy/anhydride/amine system to satisfaction.

On the basis of the previous discussion, Kamal's two-rate-constant autocatalytic model [see eq. (5)] is selected for the cure kinetics modeling of the studied epoxy resin system. The parameters of this model, K_1,

TABLE II
Kinetics Parameters for Kamal's Model of the Resin Systems

Parameters	Epon	EAS25	EAS50	EAS75
Pre-exponential constant, K_{10} (1/s)	$e^{10.75}$	$e^{13.77}$	$e^{13.73}$	$e^{17.70}$
Pre-exponential constant, K_{20} (1/s)	$e^{16.73}$	$e^{17.24}$	$e^{10.49}$	$e^{2.43}$
Activation energy, ΔE_1 (kJ/mol)	58.87	68.73	68.28	82.37
Activation energy, ΔE_1 (kJ/mol)	71.71	74.70	53.26	29.75
m	0.723	0.675	0.776	0.713
n	1.277	1.325	1.224	1.287
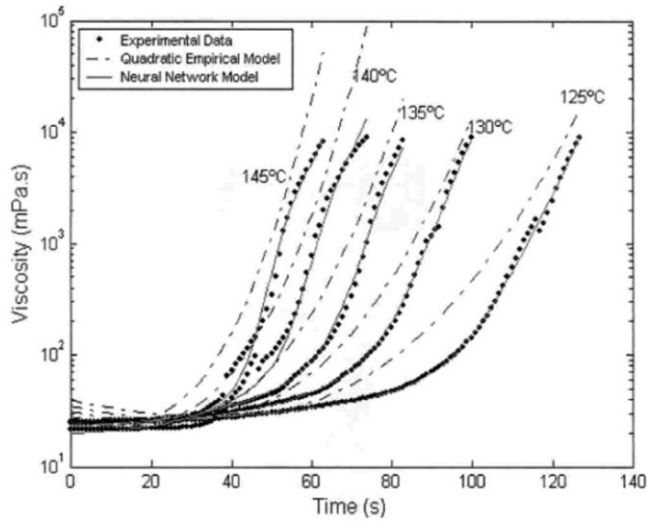
Figure 14 Comparison of experimental viscosity data with the quadratic empirical model and the neural network model at different curing temperatures for Epon.

K_2, m, and n, are determined from the isothermal DSC running data. The values of $d\alpha/dt$ are first calculated by applying eqs. (2) and (15) on the isothermal scanning data. The corresponding values of α are then calculated by applying eqs. (1), (15), and (16). Finally, the $d\alpha/dt$ versus α values are fitted with a least square curve using the Levenberg–Marquardt algorithm.

The heat flow versus time curves from the isothermal scanning measurements for the Epon resin are shown in Figure 2. Following the curve fitting procedure described above, the values of the constants in Kamal's model were obtained for the five different isothermal scanning temperatures. The m and n were found relatively insensitive to temperature, and the overall reaction order, $m + n$, can be assumed to be 2. The average values of m and n at the five different temperatures were taken as:

$$m = 0.723$$

$$n = 1.277 \tag{17}$$

The equilibrium constants K_1 and K_2 are temperature dependent following the Arrhenius relationship. The values of K_1 and K_2 at the five different tempera-

tures and the least-square fits are plotted in Figure 3. The values of K_{10}, K_{20}, ΔE_1, and ΔE_2 were found by fitting straight lines to the K_1, K_2 versus $1/T$ data points [eq. (5)]. The following values were thus obtained:

$$K_{10} = e^{10.75} \text{ S}^{-1}$$

$$K_{20} = e^{16.73} \text{ S}^{-1}$$

$$\Delta E_1 = 58.872 \text{ kJ/mol}$$

$$\Delta E_2 = 71.708 \text{ kJ/mol} \tag{18}$$

Application of eqs. (17) and (18) into eq. (5) gives the following cure kinetics expression for the Epon resin:

$$\frac{d\alpha}{dt} = \left(e^{10.75} \exp\left(-\frac{7081.16}{T} \right) + e^{16.73} \right.$$

$$\left. \times \exp\left(-\frac{8625.05}{T} \right) \alpha^{0.723} \right) (1 - \alpha)^{1.277} \tag{19}$$

where T is the absolute temperature in Kelvin.

In Figure 4, the predicted cure rate values are compared to the experimental data from the dynamic DSC runs at the four different heating rates. It can be seen that excellent agreement between the modeling results and experimental data is achieved, although the isothermal curing measurements are performed over a narrow temperature range. The kinetic behavior of the Epon resin under both isothermal and dynamic conditions can be described with the same cure kinetics model over the temperature range that covers the usual processing conditions.

Following the same modeling procedure as for the Epon, the cure kinetics of the other three soy-based epoxy resin formulations are also characterized. The DSC heat flow versus time curves of the EAS25 resin samples at different isothermal temperatures are shown in Figure 5. The values of K_1 and K_2 at the five different temperatures and the corresponding least-square fits are plotted in Figure 6. The cure kinetics of the EAS25 resin is modeled as:

$$\frac{d\alpha}{dt} = \left(e^{13.77} \exp\left(-\frac{8266.56}{T} \right) + e^{17.24} \right.$$

$$\left. \times \exp\left(-\frac{8985.00}{T} \right) \alpha^{0.675} \right) (1 - \alpha)^{1.325} \tag{20}$$

TABLE III
The Weights and Biases of the Neural Network Model for Epon

W_{1i}^h ($i = 1$–5)	W_{2i}^h ($i = 1$–5)	b_i^h ($i = 1$–5)	W_i^0 ($i = 1$–5)	b^0
−49.7201	0.1005	−3.0965	−1.4163	
−3.3133	−0.9651	83.7162	−0.0621	
−8.5356	0.1576	−15.1444	−783.7300	268.5537
8.8690	−0.2236	25.2162	200.7557	
−8.7203	0.1965	−21.3595	517.8014	

TABLE IV
Parameters for the Quadratic Empirical Equation of the Resin Systems

Parameters	Epon	EAS25	EAS50	EAS75
U (J/mol)	3.02×10^4	1.178×10^4	6.268×10^3	1.069×10^3
μ_∞ (Pa s)	4.248×10^{-6}	8.514×10^{-4}	0.1805	0.0169
a_0	1700.90	−4458.39	−461.15	463.99
a_1	−8.93	22.26	2.62	−2.026
a_2	0.0116	−0.0278	−0.003716	0.00213
b_0	−20038.58	2.945×10^4	−3718.9	−7557.87
b_1	103.45	−146.54	16.85	36.53
b_2	−0.1323	0.1825	−0.01867	−0.0439

The comparison between the model-predicted dynamic scanning curves and the experimental data is shown in Figure 7.

The DSC heat flow versus time curves of the EAS50 resin samples at different isothermal temperatures are shown in Figure 8. The values of K_1 and K_2 at the five different temperatures and the corresponding least-square fits are plotted in Figure 9. The cure kinetics of the EAS50 resin is modeled as:

$$\frac{d\alpha}{dt} = \left(e^{13.73}\exp\left(-\frac{8212.15}{T} \right) + e^{10.49} \right.$$
$$\left. \times \exp\left(-\frac{6405.49}{T} \right)\alpha^{0.776} \right)(1 - \alpha)^{1.224} \quad (21)$$

The comparison between the model-predicted dynamic scanning curves and the experimental data is shown in Figure 10.

The DSC heat flow versus time curves of the EAS75 resin samples at different isothermal temperatures are shown in Figure 11. The values of K_1 and K_2 at the five different temperatures and the corresponding least-square fits are plotted in Figure 12. The cure kinetics of the EAS75 resin is modeled as:

$$\frac{d\alpha}{dt} = \left(e^{17.70}\exp\left(-\frac{9907.59}{T} \right) + e^{2.43} \right.$$
$$\left. \times \exp\left(-\frac{3577.84}{T} \right)\alpha^{0.713} \right)(1 - \alpha)^{1.287} \quad (22)$$

The comparison between the model-predicted dynamic scanning curves and the experimental data is shown in Figure 13.

The parameters of the cure kinetics models for the four resin formulations are summarized in Table II. The performances of the fitted cure kinetics models for all the four resin formulations were highly satisfactory, justifying the suitability of Kamal's model for the soy-based resin system under the present study. Depending on the actual application, the cure kinetics of a soy-based epoxy resin with arbitrary EAS to Epon ratio (by weight) between 0 and 3 can be evaluated following the same modeling procedure described above. The cure kinetics model obtained can be used to characterize the curing process during various composite manufacturing methods, and some other important resin processing properties, such as the resin rheology.

Rheology characterization

The viscosity profile of the Epon resin, as a function of time at different temperatures, is shown in Figure 14. The viscosity increased slowly at the beginning of each curing process, and then rose faster because of crosslinking reaction. At higher temperatures, the viscosity of the resin was initially lower, but then increased earlier due to the faster curing.

Based on the extent of the viscosity measurements, the quadratic empirical equation [eq. (9)] was first selected to model the different epoxy resin systems. Equation (9) can also be written as:

$$\ln\mu = A + K_1\alpha + K_2\alpha^2 \quad (23)$$

where A is a temperature-dependent parameter defined as:

TABLE V
The Weights and Biases of the Neural Network Model for EAS25

W_{1i}^h ($i = 1$–5)	W_{2i}^h ($i = 1$–5)	b_i^h ($i = 1$–5)	W_i^0 ($i = 1$–5)	b^0
−16.8990	−0.1037	−59.8139	−1.3188	
96.2464	−0.5696	29.6780	1.4861	
−33.3310	−0.1981	40.8780	−2.2659	4.3230
9.5369	−0.04446	3.3801	0.8748	
−54.4810	−1.9095	291.9770	−0.8873	

TABLE VI
The Weights and Biases of the Neural Network Model for EAS50

W_{1i}^h ($i = 1$–5)	W_{2i}^h ($i = 1$–5)	b_i^h ($i = 1$–5)	W_i^0 ($i = 1$–5)	b^0
−3.4878	−0.3184	85.6824	−1.4844	
11.3599	−0.1262	−30.9803	2.9589	
44.2173	0.1977	−44.9342	2.2514	2.0205
11.8093	−0.04657	3.2266	0.8506	
22.8517	0.9089	44.2815	0.6425	

$$A = \ln \mu_\infty + \frac{U}{RT} \quad (24)$$

The constant K_1, K_2 and the parameter A in eq. (23) can be found as follows. First, the natural logarithm of the measured viscosity values was plotted versus the corresponding calculated values of degree of cure, α. In this plot, the values of μ and α at each point correspond to the same time and temperature. Second, the data points of μ and α at each temperature were fitted against a quadratic polynomial function with a least-squares algorithm. The values of K_1, K_2, and A are thus determined for the five temperatures.

K_1, K_2 can be found to be temperature dependent. By assuming

$$K_1 = a_0 + a_1 T + a_2 T^2$$

$$K_2 = b_0 + b_1 T + b_2 T^2 \quad (25)$$

the values of a_0, a_1, a_2, b_0, b_1, and b_2, can be obtained by curve fitting the K_1, K_2 values of the corresponding T with quadratic polynomials. Similarly, A is also temperature dependent as indicated by eq. (24). The values of A are then plotted versus $1/T$ and fitted with a least-squares straight line, which gives the values of μ_∞ and U.

By following the curve fitting procedure described above, the values of the constants in the quadratic empirical equation [eq. (9)] for Epon resin were obtained as:

$$U = 30{,}203 \text{ J/mol}$$

$$\mu_\infty = 4.25 \times 10^{-6} \text{ Pas} \quad (26)$$

$$a_0 = 1700.90; \quad b_0 = -20038.58$$
$$a_1 = -8.93; \quad b_1 = 103.45$$
$$a_2 = 0.0116; \quad b_2 = -0.1323$$

The values of the constants were substituted into eq. (9) to predict the viscosity of Epon resin as a function of time and temperature. The predicted viscosity profile is shown in Figure 14, along with the measured viscosity.

As can be seen in Figure 14, while the quadratic empirical equation gives relatively accurate viscosity prediction for high viscosity values, its performance at low viscosity stages, often the critical viscosity stages in composite process modeling, is not satisfactory. To improve the modeling accuracy, a viscosity model based on the two-layer feedforward neural network, shown in Figure 1, was developed.

The values of the weights and biases of the neural network are fully decided by the training process. The data from the experiments are processed to get the inputs and outputs for the neural network. As can be seen from the last section, the inputs to the neural network α, the degree of cure, and T, the temperature, and the output of the neural network μ, the viscosity, are what the curve fitting methods need for the acquisition of the constants values in the empirical viscosity models. Thus, the training data processing for the neural network is generally the same as for data preparation in the traditional modeling processes described above.

The different experimental data from isothermal viscosity measurements at different temperatures were then combined together to form one set of training data, including two inputs and one corresponding

TABLE VII
The Weights and Biases of the Neural Network Model for EAS75

W_{1i}^h ($i = 1$–5)	W_{2i}^h ($i = 1$–5)	b_i^h ($i = 1$–5)	W_i^0 ($i = 1$–5)	b^0
45.9333	0.002343	−22.4113	4.2299	
−8.9212	0.02890	−1.3550	−1.1609	
−35.1841	−12.0557	1642.6439	−1.2615	2.4244
−38.7583	3.8054	−516.4210	−1.3339	
−67.5688	0.2826	−3.4756	1.0769	
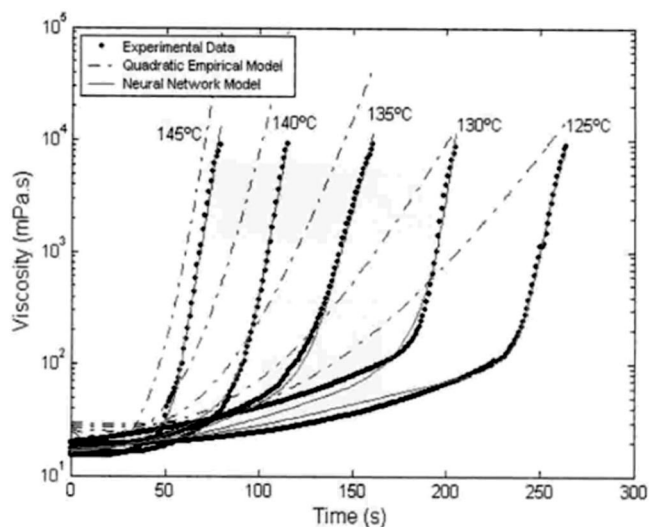
Figure 15 Comparison of experimental viscosity data with the quadratic empirical model and the neural network model at different curing temperatures for EAS25.
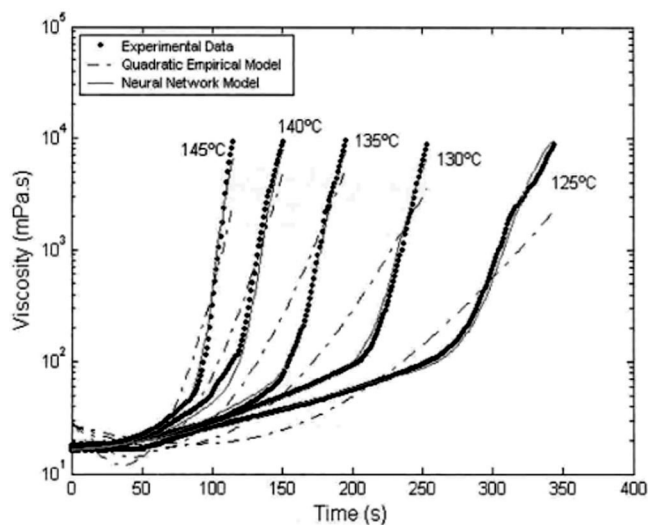

Figure 16 Comparison of experimental viscosity data with the quadratic empirical model and the neural network model at different curing temperatures for EAS50.

output, for the training of the feedforward neural network.

In this study, the neural network toolbox in MAT-LAB was used. The Levenberg–Marquardt backpropagation algorithm was chosen for the training of the neural network because it is one of the fastest training algorithms. The number of the neurons in the hidden layer was obtained by trial-and-error. By varying the initial values of the weights and biases and the number of neurons in the hidden layer, satisfactory curve fitting can be achieved and appropriate weights and biases are obtained. The values of the weights and biases of a five-neuron neural network after training are given in Table III. They are substituted into eq. (14) and the neural network-based rheology model for Epon resin was thus obtained.

The predicted viscosity profile by the neural network model is shown in Figure 14. It can be seen that the neural network model gives accurate viscosity prediction spanning the whole measurement extent. The neural network model can be readily implemented into process modeling methods, such as finite element analysis, to improve the simulation accuracy and efficiency.

Following the same procedure described above, the quadratic empirical models and the neural network-based viscosity models were also established for the other three resin formulations, EAS25, EAS50, and EAS75. The values of the constants in the quadratic empirical equation for the three soy-based epoxy resin systems are given in Table IV. The values of the weights and biases of the neural network model yielded are given in Tables V–VII, for the three resin systems, respectively. The modeling results are shown in Figures 15–17, along with the corresponding exper-

imental viscosity data. It can be seen that, for the three soy-based epoxy resins, it is also true that the neural network better models the time–temperature profiles than the empirical model.

CONCLUSIONS

The cure kinetics and rheology of a novel soy-based resin system were investigated by means of DSC and viscometer measurements. The cure kinetics of the different resin formulations was described. The effectiveness of the cure kinetic models is verified by the dynamic DSC tests at different heating rates. A Brook-
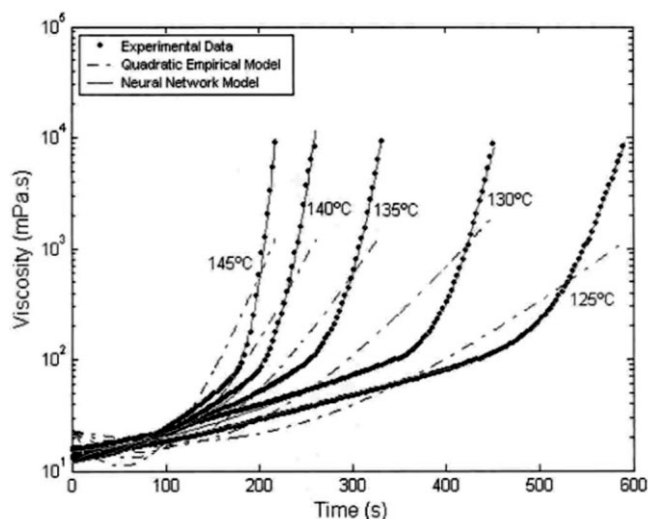
Figure 17 Comparison of experimental viscosity data with the quadratic empirical model and the neural network model at different curing temperatures for EAS75.

field viscometer with a temperature-controlling device was used to study the rheology of the soy-based resin system. A novel method based on neural network for rheology modeling is shown capable of improving modeling efficiency. The analytical models for the cure kinetics and rheology of the soy-based epoxy resin system can be readily applied into numerical modeling of various composite manufacturing processes.

References

1. Zhu, J.; Chandrashekhara, K.; Flanigan, V.; Kapila, S. J Appl Polym Sci 2004, 916, 3513.
2. Zhu, J.; Chandrashekhara, K.; Flanigan, V.; Kapila, S. Compos A 2004, 351, 95.
3. Liang, G.; Garg, A.; Chandrashekhara, K.; Flanigan, V.; Kapila, S. J Reinforced Plast Compos 2005, 24, 1509.
4. Lee, W. I.; Loos, A. C.; Springer, G. S. J Compos Mater 1982, 16, 510.
5. Dusi, M. R.; Lee, W. I.; Ciriscioli, P. R.; Springer, G. S. J Compos Mater 1987, 21, 243.
6. Shanku, R.; Vaughan, J. G.; Roux, J. A. Adv Polym Technol 1997, 16, 297.
7. Hubert, P.; Johnson, A.; Poursartip, A.; Nelson, K. In 46th International SAMPE Symposium, Long Beach, CA, May 2001; p 2341.
8. Mantell, S. C.; Ciriscioli, P. R.; Almen, G. J Reinforced Plast Compos 1995, 14, 847.
9. Kim, J.; Moon, T. J.; Howell, J. R. J Compos Mater 2001, 36, 2479.
10. Ivankovic, M.; Incarnato, L.; Kenny, J. M.; Nicolais, L. J Appl Polym Sci 2003, 90, 3012.
11. Charchad, Y. R.; Roux, J. A.; Vaughan, J. G. J Reinforced Plast Compos 1995, 14, 495.
12. Valliappan, M.; Roux, J. A.; Vaughan, J. G. J Reinforced Plast Compos 1996, 15, 295.
13. Kim, D. H.; Han, P. G.; Jin, G. H.; Lee, W. I. J Compos Mater 1997, 31, 2105.
14. Yoo, Y. E.; Lee, W. I. Polym Compos 1996, 17, 368.
15. Lee, C. L.; Wei, K. H. J Appl Polym Sci 2000, 77, 2139.
16. Kamal, M. R. Polym Eng Sci 1974, 14, 231.
17. Cole, K. C. Macromolecules 1991, 24, 3093.
18. Kenny, J. M.; Apicella, A.; Nicolais, L. Polym Eng Sci 1989, 29, 973.
19. Williams, M. L.; Landel, R. F.; Ferry, J. D. J Am Chem Soc 1955, 77, 3701.
20. Anderson, J. A.; Rosenfeld, E., Eds. Neurocomputing: Foundations of Research; MIT Press: Cambridge, MA, 1988.
21. Lau, C. Neural Networks: Theoretical Foundations and Analysis; IEEE Press: New York, 1992.
22. Rodriguez, F.; Jaramillo, N. B.; Pandya, N. In Intelligent Engineering Systems through Artificial Neural Networks; Dagli, C.; Akay, E.; Philip Chen, C. L.; Fernandez, B. R.; Gosh, J., Eds.; ASME Press: New York, 1996; Vol. 6, p 533.
23. Hussain, M. A. Artif Intell Eng 1999, 13, 55.
24. Zeng, P. Appl Mech Rev 1998, 51, 173.
25. Funahashi, K. I. Neural Netw 1989, 2, 183.
26. Hornik, K.; Stinchcombe, M.; White, H. Neural Netw 1989, 2, 359.
27. Ito, Y. Neural Comput 1994, 6, 1233.
28. Woo, E. M.; Seferis, J. C. J Appl Polym Sci 1990, 40, 1237.
29. Khanna, U.; Chanda, M. J Appl Polym Sci 1993, 49, 319.